ARTICLES

Structural insights into the evolutionary paths of oxylipin biosynthetic enzymes

Dong-Sun Lee[1]*, Pierre Nioche[2]*, Mats Hamberg[3] & C. S. Raman[1]

The oxylipin pathway generates not only prostaglandin-like jasmonates but also green leaf volatiles (GLVs), which confer characteristic aromas to fruits and vegetables. Although allene oxide synthase (AOS) and hydroperoxide lyase are atypical cytochrome P450 family members involved in the synthesis of jasmonates and GLVs, respectively, it is unknown how these enzymes rearrange their hydroperoxide substrates into different products. Here we present the crystal structures of *Arabidopsis thaliana* AOS, free and in complex with substrate or intermediate analogues. The structures reveal an unusual active site poised to control the reactivity of an epoxyallylic radical and its cation by means of interactions with an aromatic π-system. Replacing the amino acid involved in these steps by a non-polar residue markedly reduces AOS activity and, unexpectedly, is both necessary and sufficient for converting AOS into a GLV biosynthetic enzyme. Furthermore, by combining our structural data with bioinformatic and biochemical analyses, we have discovered previously unknown hydroperoxide lyase in plant growth-promoting rhizobacteria, AOS in coral, and epoxyalcohol synthase in amphioxus. These results indicate that oxylipin biosynthetic genes were present in the last common ancestor of plants and animals, but were subsequently lost in all metazoan lineages except Placozoa, Cnidaria and Cephalochordata.

Oxylipins are bioactive lipids derived from oxygenation of polyunsaturated fatty acids. Both jasmonates[1–4] and GLVs[5,6] are representative plant oxylipins. Whereas jasmonates are essential for plant development and host immunity[7–9], GLVs are released to counter biotic and abiotic stresses, such as wounding, herbivore attacks and ozone exposure[10]. Curiously, jasmonates and animal prostaglandins[11,12] share notable structural and functional properties (Supplementary Figs 1 and 2).

AOS[13–18] catalyses the first committed step[19] in the synthesis of jasmonates, and hydroperoxide lyase (HPL)[5,20,21] generates GLVs (Fig. 1). Some plants use divinyl ether synthase (DES) to produce divinyl ethers[22,23], which are thought to have a role in host defense. AOS, HPL, and DES belong to the cytochrome P450 (P450 or CYP) superfamily[16,24], which currently has more than 8,700 members distributed across all three domains of life. All P450 enzymes are thiolate-coordinated haem proteins and most of them function as monooxygenases[25]. Although there is <20% sequence identity within the superfamily, P450s share a common protein fold, as shown by nearly 30 unique crystal structures of bacterial and human enzymes[26,27]. However, there is no structural information on plant P450s.

AOS, HPL and DES are members of the CYP74 family. These unusual P450s do not function as monoooxygenases, but instead rearrange fatty acid hydroperoxides into structurally different products (Fig. 1). Despite four decades of research, several observations concerning CYP74 biochemistry and catalysis have remained enigmatic. Here we present the crystal structure of *A. thaliana* AOS (At-AOS, also known as CYP74A) and illustrate how an important new activity evolved. We also show that a single substitution changes the product specificity of AOS to that of an HPL. Finally, we report that CYP74 enzymes are not confined to plants, but also occur in bacteria and animals.

Overall structure of AOS

At-AOS adopts the characteristic fold of P450s (Fig. 2a, Supplementary Tables 1 and 2, and Supplementary Fig. 3). The membrane-binding region can be identified by bound detergent molecules and by its rather extensive non-polar surface (~2,400 Å^2; Fig. 2a and Supplementary

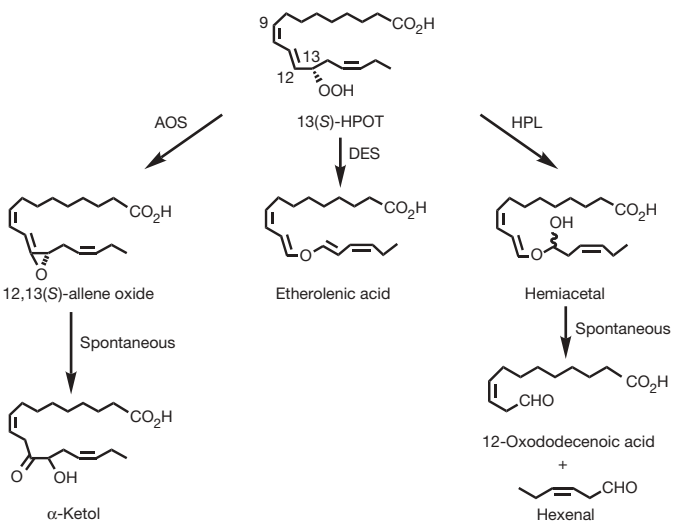

Figure 1 | Reactions catalysed by the CYP74 enzyme family. In higher plants, C_{18} fatty acids (linoleic and linolenic acids) are oxygenated at either position 9 or 13 by lipoxygenases to yield hydroperoxides. Subsequently, these are converted by allene oxide synthase (AOS, also known as CYP74A), hydroperoxide lyase (HPL, also known as CYP74B) and divinyl ether synthase (DES, also known as CYP74D) to allene oxide (an essential intermediate in jasmonate biosynthesis), green leaf volatiles (aldehydes) and divinyl ethers, respectively. For clarity, only 13-hydroperoxide-derived metabolites are shown. 12,13(*S*)-allene oxide, 12,13*S*-epoxy-9*Z*,11,15*Z*-octadecatrienoic acid; 13(*S*)-HPOT, 13*S*-hydroperoxyoctadecatrienoic acid; α-ketol is the hydrolytic product of the highly unstable allene oxide; hemiacetal, hydroxyhexenyloxydodecadienoic acid.

[1]Department of Biochemistry and Molecular Biology, University of Texas Medical School, Houston, Texas 77030, USA. [2]Université Paris Descartes, INSERM UMR-S 747, 75270 Paris cedex 06, France. [3]Division of Physiological Chemistry II, Department of Medical Biochemistry & Biophysics, Karolinska Institutet, S-17177 Stockholm, Sweden.
*These authors contributed equally to this work.

Fig. 4a, b). It also harbours the entry point for the 22-Å deep substrate access channel (Supplementary Fig. 4c). AOS lacks the characteristic amino-terminal transmembrane domain of microsomal P450s[28] and, yet, associates very tightly with chloroplastic envelope membranes[29] and plastoglobules[30]. A comparison of the crystal structures of At-AOS and mammalian CYP2C5 (ref. 28) reveals that both P450s use the same macromolecular surface to interact with the membrane (Supplementary Fig. 5).

The haem cofactor of At-AOS is inserted between the I-helix and the L-helix and, like classical P450s[26,27], its propionate groups interact with strictly conserved basic residues through hydrogen bonds (Fig. 2b). Haem is in the low-spin state, with Cys 471 and a water molecule serving as proximal and distal coordination ligands of Fe(III), respectively (Fig. 2b and Supplementary Fig. 6a). However, there are three major changes that distinguish At-AOS from all other known P450 structures. First, nine residues are inserted into the middle of the signature haem-binding loop harbouring the Cys 471 ligand (Fig. 2c, Supplementary Fig. 6b and Supplementary Discussion). This is extraordinary because even a single residue insertion within this region is not observed in >8,000 P450s. This modification, which is preserved in all CYP74 family members, not only alters the proximal site topology but also causes extensive remodelling of the macromolecular surface essential for redox partner interactions in typical P450s (Supplementary Fig. 6c). In addition, the Fe–S bond length is reproducibly longer (2.4 Å versus 2.2 Å) in the substrate-free state. Second, the kink centred on the second glycine of the I-helix (A/G)GxxT motif[26] in classical P450s is shifted by three residues towards the N terminus and is now localized on Asn 321, positioning the amide group directly above the haem iron (4.4 Å; Fig. 2b and Supplementary Fig. 6d). Third, Ile 328 substitutes for the I-helix Thr that is critical for mediating proton delivery to haem-bound dioxygen in conventional P450s[26,27]. Together, these structural modifications preclude monooxygenase activity in AOS. Notably, hydroperoxide-using CYP74 may have been an evolutionary intermediate during the transition from H_2O_2 (ref. 31) to O_2 as oxygen donor in P450 catalysis (Supplementary Figs 7–9 and Supplementary Discussion).

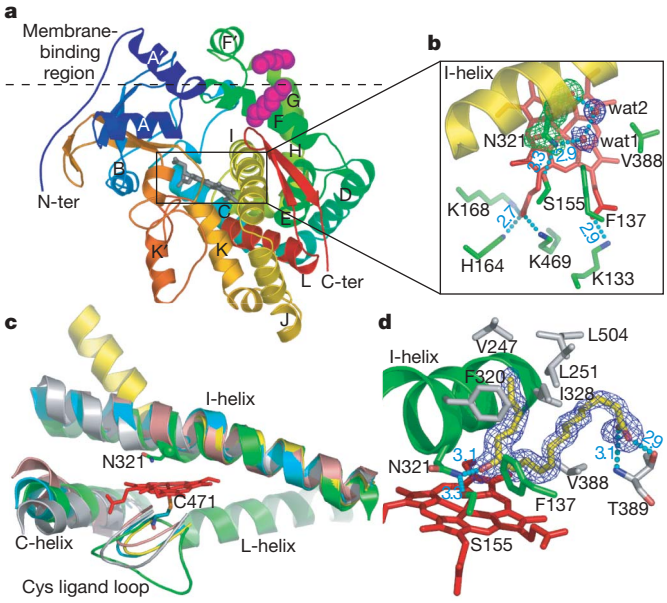

Figure 2 | Tertiary topology and substrate binding site of AOS. a, Ribbon diagram of At-AOS, rainbow-coloured from the N terminus (N-ter, blue) to the C terminus (C-ter, red). van der Waals representation (magenta) identifies hydrophobic tails of two detergent molecules interacting with F, F′ and G helices, which are part of the membrane-associated nonpolar surface. Regions above and below the dashed line are facing the membrane and cytosol, respectively. **b**, Close-up view of the haem (red) environment. $F_o - F_c$ simulated annealing omit electron density (contoured at 3σ) is shown for Asn 321 (green) and two water molecules (wat1 and wat2, blue). **c**, Superposition of structural elements in AOS (green), CYP102A1 (pink, PDB ID: 1BVY), CYP3A4 (blue, PDB ID: 1TQN), CYP51 (yellow, PDB ID: 1EA1) and CYP152B1 (grey, PDB ID: 1IZO). **d**, Active site configuration. $F_o - F_c$ simulated annealing omit electron density (countoured at 3σ) of 13(*S*)-HOT (blue). Cyan dotted lines represent hydrogen bonds (donor–acceptor distances are in Å).

Identifying active site interactions

To gain insight into the structural basis of substrate recognition, we crystallized AOS together with 13(*S*)-HOT, a close mimic incorporating OH instead of the OOH group (Supplementary Fig. 10a). The structure shows well-defined electron density for both the fatty acid and the hydroxy portions of the molecule (Fig. 2d and Supplementary Video 1). 13(*S*)-HOT nicely conforms to the shape and physicochemical properties of the AOS active site. Its hydroxyl oxygen takes the place of a water molecule (wat1, Fig. 2b) in the substrate-free structure and interacts with the amide side chain of Asn 321 by a hydrogen bond. The carboxyl group engages in hydrogen bonding with Thr 389, and the aliphatic segments maintain favourable hydrophobic contacts with neighbouring non-polar side chains. This binding mode explains why both diatomic (CO) and other axial haem ligands that attempt to coordinate the iron in a linear fashion experience difficulties due to the positioning of the carboxamide directly above the haem plane. Conversely, the peroxy group of the substrate approaches from the side and successfully ligates the haem while having a productive interaction with the catalytic Asn 321. Mutating Asn 321 abolishes >95% of the enzyme activity (Supplementary Fig. 10b).

Next we co-crystallized AOS with 12*R*,13*S*-vernolic acid, an analogue of the putative epoxyallylic reaction intermediate in AOS catalysis[17] (Supplementary Fig. 10a). Our structure illustrates that the binding mode of 12*R*,13*S*-vernolic acid is very similar to that of 13(*S*)-HOT, with C11 residing in proximity to the aromatic face of Phe 137 (Fig. 3a and Supplementary Fig. 10c). Furthermore, our sequence analysis showed that whereas Phe 137 is strictly conserved in AOS, a Leu takes its place in HPL and DES (Supplementary Fig. 10d). Because enzymological studies[17] have proposed that C11 is the site of both radical and carbocation formation, we hypothesized that removal of the electron-rich aromatic ring of Phe 137 would affect catalysis. Consistent with our prediction, At-AOS(F137L) is severely compromised in its ability to generate allene oxide (Fig. 3b). These observations identify an essential role for Phe 137. It is poised to stabilize the carbon-centred radical and to interact with the incipient carbocation by means of cation–π interactions (Supplementary Discussion).

Single point mutation confers HPL activity to AOS

We reasoned that, if the inability to stabilize a carbon-centred radical at C11 is the sole reason for loss of AOS activity, then the F137L mutant is likely to have altered product specificity. To test this, we probed for HPL and DES metabolites and found that At-AOS(F137L) exhibits robust HPL activity (Fig. 3b). However, DES products were not detected. To evaluate the molecular consequences of this mutation, we solved the structure of At-AOS(F137L) in complex with 12*R*,13*S*-vernolic acid (Fig. 3c and Supplementary Video 2) or with 13(*S*)-HOD (Supplementary Fig. 11a–d). The binding mode of both compounds is quite similar to that in the wild-type enzyme (Supplementary Fig. 11c, d). Notably, Phe has a bulkier side chain compared to Leu, but it is >5 Å away from the haem iron (Supplementary Fig. 11e), and therefore it is incapable of altering the reaction mechanism by means of steric effects.

Because our homology model of tomato HPL (Fig. 3c, grey overlay) and bioinformatic analysis showed that Ser 155 is substituted by an Ala in HPL (Supplementary Fig. 10d), we constructed the double mutant At-AOS(F137L,S155A) and found it to exhibit even stronger

HPL activity. It converted the hydroperoxides 13(*S*)-HPOD, 13(*S*)-HPOT, 9(*S*)-HPOD and 11(*S*)-HPHT into the corresponding HPL products to a varying extent (Supplementary Fig. 12). Concerning the two first-mentioned hydroperoxides, 13(*S*)-HPOT gave a lower ratio of HPL/AOS products (approximately 25:75) than did 13(*S*)-HPOD (approximately 85:15). Structural analysis of the enzyme-bound 13(*S*)-HOT reveals that the C15 double bond is 3.3 Å away from C11, and it seems possible that the diminished effect of the F137L substitution on the formation of HPL products in the 13(*S*)-HPOT case can be attributed to a Phe-137-independent stabilization of the epoxyallylic intermediate by means of anchimeric assistance by π electrons from the C15=C16 double bond (Supplementary Fig. 13).

We also demonstrate that AOS to HPL conversion works across evolutionary boundaries. Although the eudicot (*Arabidopsis*) and monocot (*Oryza sativa*) branches of angiosperms diverged 140–180 million years ago[32], introduction of F92L substitution into one of the two AOS genes found in rice (Supplementary Fig. 10d) readily changes product specificity (Supplementary Figs 14 and 15, and Supplementary Table 3).

Overall, we have established that AOS sandwiches C11 in between two π systems to ensure that 13(*S*)-HPOT, the only substrate that will yield jasmonates, is efficiently converted to allene oxide. Conversely, the HPL active site facilitates radical rearrangement by excluding a strategically positioned aromatic residue in the vicinity of C11 (Supplementary Discussion).

Structural mechanism for CYP74 catalysis

In both AOS and HPL, the terminal hydroperoxide oxygen of the substrate coordinates the ferric haem iron (**2**) (Fig. 4) after displacing two bound water molecules (wat1 and wat2; see (**1**) and Fig. 2b) from the active site. With electrostatic assistance from a carboxamide (Supplementary Discussion), O−O homolysis[33] ensues, giving rise to an alkoxyl radical (RO•) and a protonated ferryl species (S−Fe(IV)−OH) (**3**) (Fig. 4). RO•, while maintaining a hydrogen bond with the amide, adds to a proximate double bond (C11=C12) to generate an epoxide and a carbon-centred radical (C•) at C11 (**4**). Hydrogen bonding to RO• will favour cyclization over allylic hydrogen abstraction (Supplementary Discussion). The two mechanisms diverge at this stage. In the case of AOS, oxidation of

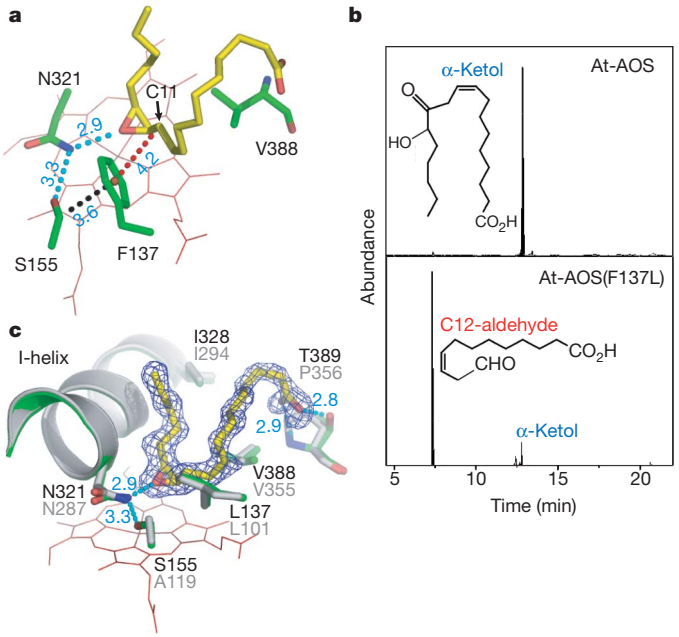

Figure 3 | Structural basis for evolving HPL activity from the AOS scaffold. **a**, At-AOS complexed with the reaction intermediate analogue (–)-vernolic acid (yellow). **b**, At-AOS(F137L) exhibits HPL activity. Recombinant wild-type and AOS(F137L) (0.2–4 μM) were stirred with 13(*S*)-HPOD (200 μM) at 23 °C for 15 min. After derivatization, product profiles were determined using gas chromatography–mass spectrometry (GC–MS) analysis with authentic compounds serving as references. The top panel shows At-AOS catalysed conversion to α-ketol (13-hydroxy-12-oxo-9*Z*-octadecenoic acid, *m*/*z* 412), the hydrolytic product of allene oxide. AOS(F137L) yielded 12-oxo-9*Z*-dodecenoic acid (C12-aldehyde, *m*/*z* 224), the product of HPL catalysis, as the major component (bottom panel). **c**, At-AOS(F137L) bound to (–)-vernolic acid (yellow) reveals the catalytic site structure of HPL. $F_o - F_c$ simulated annealing omit electron density, contoured at 3σ, is shown in blue for the ligand. The homology model of tomato HPL (grey) is superimposed.

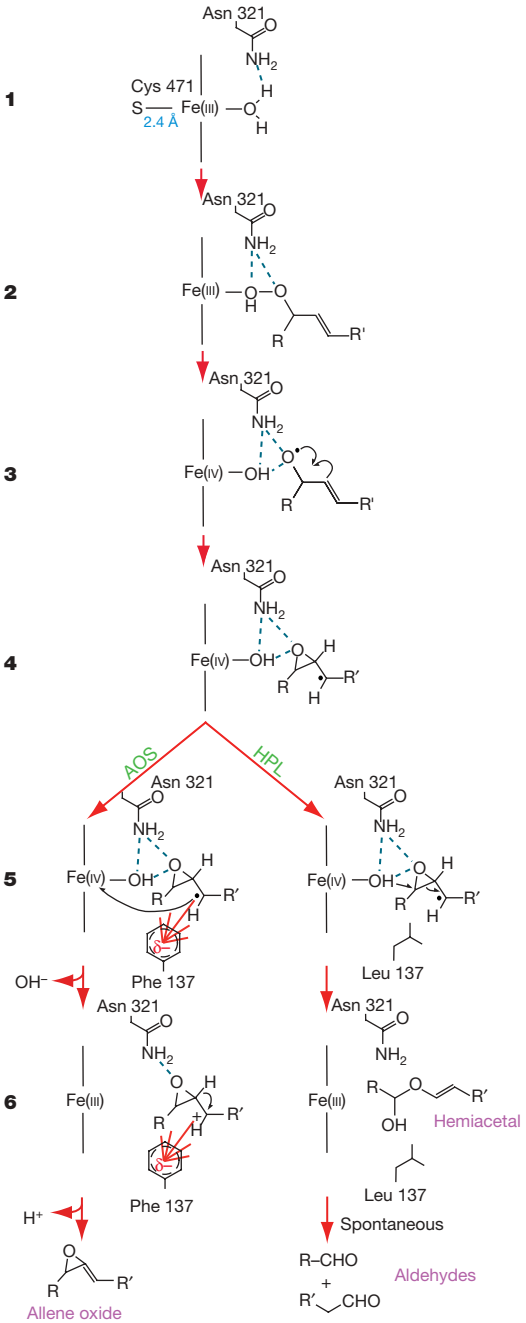

Figure 4 | Proposed reaction paths for AOS and HPL on the basis of the current structural and enzymological studies[14–17,21]. The intermediate epoxyallylic radical formed in step **4** can either undergo one electron oxidation followed by proton loss (AOS) or oxygen rebound (HPL). The structure of the peroxide substrate is abbreviated to highlight the region undergoing chemical transformation. For clarity, the Fe–S bond between the haem iron and Cys 471 is only shown in step **1**. It remains intact throughout the catalytic cycle. Hydrogen bonds are illustrated with blue dashed lines.

C• by S−Fe(IV)−OH (**5**, left) is made possible by Phe 137, which also stabilizes the incipient carbocation (C^+) (at C11; **6**, left) by means of cation–π interactions. On β-proton elimination, a C=C bond is introduced adjacent to the epoxide, and allene oxide is generated (Supplementary Discussion). In the case of HPL there are two fundamental differences. First, electron transfer does not occur owing to difficulty in stabilizing the radical at this position. Consequently, the epoxycarbinyl radical undergoes C–C scission[34], yielding a radical at C13 that is able to oxygen rebound (iron-catalysed oxygen transfer involving radical recombination) (**5**, right) given the proximity to the ferryl centre (3.3 Å; Supplementary Fig. 11e). Second, the lack of a Phe 137 equivalent in HPL (**5**, right) prevents a carbocation intermediate from being adequately enriched or stabilized at C11. These conditions promote the formation of an unstable hemiacetal[21], which spontaneously dissociates into short-chain aldehydes (**6**, right). In the case of DES, subtle alterations (Supplementary Fig. 16) may be sufficient for disabling oxygen rebound in favour of stereospecific hydrogen abstraction[24] by the protonated ferryl centre.

Although the CYP74 enzymes have evolved by precluding monooxygenation chemistry, they have used remarkable strategies to utilize the peroxide shunt pathway[33] and to exquisitely control the reactivity of catalytic intermediates for achieving product specificity. Nevertheless, our structural mechanism has both similarities and differences with the consensus hydroxylation mechanism of P450 monooxygenases[35]. The protonated ferryl centre, S−Fe(IV)−OH (**3**), is a common intermediate in both systems. In the case of CYP74, a nine-residue insertion in the proximal Cys loop contributes significantly to diminishing the donor strength of the thiolate (Fig. 2c), favouring the generation of S−Fe(IV)−OH complex that can readily participate in electron transfer (AOS) or oxygen rebound (HPL). Conversely, for P450 monooxygenases[36], robust electron donation (push) from the proximal thiolate to the haem iron allows the ferryl-porphyrin cation radical (S−Fe(IV)=O + •) to abstract a hydrogen atom from the substrate. The highly reactive S−Fe(IV)−OH ($pK_a > 8.2$) generated goes on to hydroxylate the substrate radical (Supplementary Discussion). The strong push effect of the thiolate also prevents S−Fe(IV)−OH from serving as a good electron acceptor[37].

Finally, we sought to compare the active sites of CYP74 and coral catalase-like AOS (cAOS)[38,39] because of their ability to catalyse equivalent reactions (Supplementary Figs 1 and 17). We found that both systems control the reactivity of their haem cofactor in different ways to achieve the same end point (Supplementary Discussion).

Evolutionary history of oxylipin biosynthetic enzymes

On the one hand, cAOS has been found only in corals[38,40] and in a cyanobacterium[41] as a haem protein that is carboxy-terminally fused to a lipoxygenase (cAOS–LOX). On the other, the CYP74 family is thought to be a plant invention[42] because it has not been identified outside of angiosperms and moss[24]. These observations raise three important questions. Is CYP74 unique to *Plantae*? Are these two allene oxide-generating protein families mutually exclusive in the same organism? And, could they have evolved independently and simultaneously?

Because several groups[18,40] have failed to detect CYP74 in animals by means of homology-based polymerase chain reaction cloning, we took a structure-guided approach. By combining insights from At-AOS structure with multiple sequence alignments, we generated three unique motifs (Supplementary Table 4) for probing genome databases. Our search yielded more than 25 potential hits in marine invertebrates and 2 in rhizobacteria (Supplementary Fig. 18). Most of them show less than 30% sequence identity with the plant CYP74 family and fall short of the 40% identity required for being classified as *bona fide* CYP74 under the current P450 nomenclature system. However, they all retain the characteristic nine-residue insert in the proximal Cys loop, the amino acid makeup of which is notably similar to that found in plant CYP74 (Supplementary Figs 19 and 20). Next, we cloned and overexpressed CYP74-like proteins from *Methylobacterium nodulans* (Mn), *Acropora palmata* (Ap; Elkhorn coral) and *Branchiostoma floridae* (Bf; amphioxus) (Supplementary Figs 21–23). Mn-CYP74 and Ap-CYP74 show HPL and AOS activities, respectively (Fig. 5). Bf-CYP74 exhibits previously unknown epoxyalcohol synthase (EAS) activity by transforming the naturally occurring 13*S*-HPOD into a *cis*-epoxide product (Fig. 5). This is distinct from flaxseed AOS-catalysed[17] conversion of an unnatural fatty acid hydroperoxide into an epoxyalcohol, where a *trans*-epoxide is generated. Although our homology models (Supplementary Fig. 24) show that the catalytic Phe is found in all three cases, we can surmise from the product profiles that it is suitably oriented for stabilizing the reaction intermediates only in Ap-AOS and Bf-EAS. The aromatic π-cloud is not in a position to influence the reaction path in Mn-HPL. This may also be the case with HPL from moss (Supplementary Fig. 18), which diverged from angiosperms over 400 million years ago[43]. Thus, it is possible that an ancestral CYP74 may have functioned as a HPL before gene duplication and neofunctionalization.

Next, we examined the genetic context of CYP74 and uncovered five remarkable features. First, there are multiple CYP74 genes in animals. Amphioxus has 20, whereas *Nematostella* has just 2 (Fig. 6). This is also true in plants; grapevine and *Arabidopsis* encode 6 and 2 genes, respectively. Second, animal CYP74 genes contain numerous introns (Supplementary Table 5). In contrast, most of the plant CYP74 genes are intronless. Third, sea anemone and *Trichoplax* CYP74 genes propagate as tandem arrays (Supplementary Fig. 25). By querying the plant genomes, we discovered that grapevine, poplar and rice CYP74 genes also do the same. Fourth, a LH2 domain is appended to the C terminus of some amphioxus CYP74, such as Bf-EAS (Supplementary Fig. 26). This domain is also located in cAOS–LOX, between the cAOS

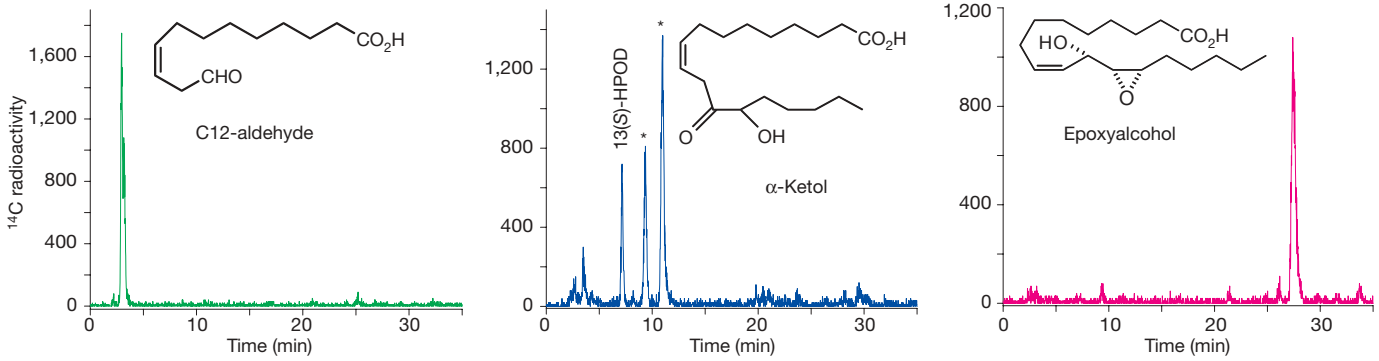

Figure 5 | Discovery of CYP74 in bacteria and animals. Recombinant CYP74 proteins from *M. nodulans* (left panel), *A. palmata* (middle panel) and *B. floridae* (right panel) were incubated with [1-^{14}C]13(*S*)-HPOD (200 μM) at 23 °C for 15 min. After derivatization, radio-HPLC was used to quantify product formation. *M. nodulans* and *A. palmata* enzymes generated C12-aldehyde and α-ketol, respectively. Peaks marked by an asterisk correspond to the *syn*/*anti* isomers of α-ketol. *B. floridae* CYP74 catalysed the formation of epoxyalcohol (12*R*,13*S*-epoxy-11*S*-hydroxy-9*Z*-octadecenoic acid). The latter is the 11*S*-hydroxy derivative of (–)-vernolic acid, whose mode of interaction with At-AOS is shown in Fig. 3a.

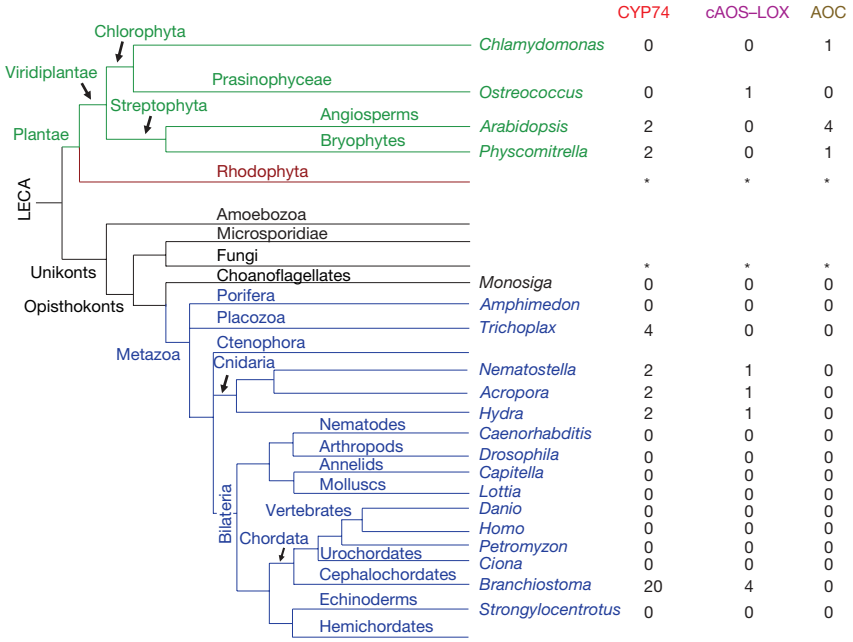

Figure 6 | Common ancestry of oxylipin biosynthetic enzymes. Lineage-specific expansion of CYP74, cAOS–LOX and AOC genes is shown (left panel). CYP74 collectively refers to fatty-acid-hydroperoxide-metabolizing non-monooxygenase cytochrome P450 family members that incorporate both a nine-residue insert in the proximal Cys ligand loop and the active site residues of At-AOS. There are 20 CYP74 genes in amphioxus, but only 4 that encode cAOS–LOX (right panel). A zero indicates that the gene was not found in the specified organism. An asterisk denotes the ability to biosynthesize jasmonic acid, but we have been unable to locate CYP74 or AOC genes in the available rhodophyte and fungal genomes (Supplementary Discussion). LECA, last eukaryotic common ancestor.

and LOX coding regions (see below). Fifth, Mn-HPL is N-terminally fused to a cyclooxygenase-like (COX-like) gene (Supplementary Figs 27–29 and Supplementary Discussion).

We investigated whether CYP74 and cAOS–LOX coexist. We identified both genes in cnidarians and cephalochordates (Fig. 6 and Supplementary Figs 30 and 31). Of the four cAOS–LOX paralogues found in the latter, one resembles the *Anabaena* enzyme (His ligand)[41], another is similar to coral cAOS (Tyr ligand)[38] and the remaining two are new. We also obtained evidence to suggest that cAOS–LOX arose from a gene fusion event. In *Plesiocystis pacifica*, cAOS and LOX are encoded by two separate genes that form an operon (Supplementary Fig. 31). Because a long-chain polyunsaturated fatty acid (C20:4) is produced by this marine myxobacterium (Supplementary Discussion), it may serve as the substrate for generating allene oxide. Although we could not find an allene oxide cyclase (AOC) (Supplementary Fig. 1) orthologue in *P. pacifica*, we located it in other myxobacteria, including in *Stigmatella aurantiaca* (Supplementary Figs 32 and 33). However, the latter does not encode CYP74 genes.

Together, our phylogenetic analysis indicates that CYP74 was present in the last common ancestor of plants and animals (Fig. 6). CYP74 genes persist in plants and in basal extant animals, including *Trichoplax*, corals, hydra and sea anemone. Even though they experienced considerable expansion in the most basal chordate (amphioxus), they were lost in vertebrates and their closest invertebrate relatives (tunicates). The propagation of these genes as multiple-copy clusters also suggests that a duplication event may have occurred in the ancestral CYP74 before the divergence of plants and animals (Supplementary Discussion). The coexistence of cAOS–LOX and CYP74 has been preserved in the cnidarian and cephalochordate lineages, but was eliminated during placozoan evolution. This illustrates that both genes were present in an animal before the cnidarian–bilaterian split[44], which occurred approximately 600 million years ago.

What is the physiological significance of CYP74 activity in bacteria and animals? This is the first time a GLV biosynthetic enzyme has been found in bacteria. Because *Methylobacterium* strains contribute to enhancing the flavour of strawberries[45], our discovery of Mn-HPL has direct implications for understanding how plant-growth-promoting rhizobacteria[46,47] mediate their actions. Notably, *M. nodulans* is a root-nodule-forming and nitrogen-fixing symbiont of *Crotalaria* species[48], the methylotrophic metabolism of which has been shown to promote optimal plant growth[49]. At this time, we are unable to establish whether bacterial HPL was acquired by means of horizontal gene transfer from plants (Supplementary Discussion). Where animals are concerned, coexistence of cAOS–LOX and AOS in *Acropora* suggests that they are part of different biosynthetic pathways. Also, the catalytic activity of Bf-EAS is reminiscent of epoxyalcohol formation from arachidonic acid by means of the 12*R*-LOX–eLOX3 pathway[50] in mammals. Related to this, we have established that C18 polyunsaturated fatty acids are abundant in amphioxus (Supplementary Table 6). Therefore, substrate availability is not an issue for the animal CYP74 enzymes. More interestingly, we have identified a leukotriene A4 hydrolase orthologue in animals that harbour CYP74 genes (Supplementary Fig. 34 and Supplementary Discussion). This lends additional support for fatty acid epoxide metabolism in marine invertebrates.

This paper explains how unusual cytochrome P450 enzymes convert fatty acid hydroperoxides into a broad spectrum of molecules that have beneficial applications in agriculture and medicine. It provides essential information for genetically modifying GLV biosynthesis to, among other things, enhance crop plants' resistance against biotic and abiotic stresses, fine-tune bitterness intensity in virgin olive oils, alter floral, fruit and vegetable flavours, and dissect plant volatile signalling mechanisms (Supplementary Discussion). In addition, it opens new vistas for understanding how biofertilizers work, as well as for exploring the biological functions of products derived from animal CYP74 enzymes.

METHODS SUMMARY

The At-AOS structure was determined by multiwavelength anomalous dispersion methods using selenomethionine-labelled protein. Difference Fourier techniques were used to solve the structures of the mutants as well as the complexes. Product formation in enzyme-catalysed reactions was assessed by gas-chromatography/mass spectrometry and radio-HPLC.

Full Methods and any associated references are available in the online version of the paper at www.nature.com/nature.

Received 14 November 2007; accepted 1 August 2008.
Published online 20 August 2008.

1. Liechti, R. & Farmer, E. E. Jasmonate biochemical pathway. *Sci. STKE* **2006**, cm3 (2006).
2. Liechti, R., Gfeller, A. & Farmer, E. E. Jasmonate signaling pathway. *Sci. STKE* **2006**, cm2 (2006).
3. Wasternack, C. Jasmonates: an update on biosynthesis, signal transduction and action in plant stress response, growth and development. *Ann. Bot. (Lond.)* **100**, 681–697 (2007).

4. Flescher, E. Jasmonates in cancer therapy. *Cancer Lett.* **245,** 1–10 (2007).
5. Matsui, K. Green leaf volatiles: hydroperoxide lyase pathway of oxylipin metabolism. *Curr. Opin. Plant Biol.* **9,** 274–280 (2006).
6. Baldwin, I. T., Halitschke, R., Paschold, A., von Dahl, C. C. & Preston, C. A. Volatile signaling in plant–plant interactions: ''talking trees'' in the genomics era. *Science* **311,** 812–815 (2006).
7. Xie, D. X., Feys, B. F., James, S., Nieto-Rostro, M. & Turner, J. G. COI1: an *Arabidopsis* gene required for jasmonate-regulated defense and fertility. *Science* **280,** 1091–1094 (1998).
8. Li, L. *et al.* The tomato homolog of CORONATINE-INSENSITIVE1 is required for the maternal control of seed maturation, jasmonate-signaled defense responses, and glandular trichome development. *Plant Cell* **16,** 126–143 (2004).
9. Kessler, A., Halitschke, R. & Baldwin, I. T. Silencing the jasmonate cascade: induced plant defenses and insect populations. *Science* **305,** 665–668 (2004).
10. Gershenzon, J. Plant volatiles carry both public and private messages. *Proc. Natl Acad. Sci. USA* **104,** 5257–5258 (2007).
11. Funk, C. D. Prostaglandins and leukotrienes: advances in eicosanoid biology. *Science* **294,** 1871–1875 (2001).
12. Keirse, M. J. Natural prostaglandins for induction of labor and preinduction cervical ripening. *Clin. Obstet. Gynecol.* **49,** 609–626 (2006).
13. Zimmerman, D. C. A new product of linoleic acid oxidation by a flaxseed enzyme. *Biochem. Biophys. Res. Commun.* **23,** 398–402 (1966).
14. Hamberg, M. Mechanism of corn hydroperoxide isomerase: detection of 12,13(*S*)-oxido-9(*Z*),11-octadecadienoic acid. *Biochim. Biophys. Acta* **920,** 76–84 (1987).
15. Brash, A. R., Baertschi, S. W., Ingram, C. D. & Harris, T. M. Isolation and characterization of natural allene oxides: unstable intermediates in the metabolism of lipid hydroperoxides. *Proc. Natl Acad. Sci. USA* **85,** 3382–3386 (1988).
16. Song, W. C. & Brash, A. R. Purification of an allene oxide synthase and identification of the enzyme as a cytochrome P-450. *Science* **253,** 781–784 (1991).
17. Song, W. C., Baertschi, S. W., Boeglin, W. E., Harris, T. M. & Brash, A. R. Formation of epoxyalcohols by a purified allene oxide synthase. Implications for the mechanism of allene oxide synthesis. *J. Biol. Chem.* **268,** 6293–6298 (1993).
18. Tijet, N. & Brash, A. R. Allene oxide synthases and allene oxides. *Prostaglandins Other Lipid Mediat.* **68–69,** 423–431 (2002).
19. Park, J. H. *et al.* A knock-out mutation in allene oxide synthase results in male sterility and defective wound signal transduction in *Arabidopsis* due to a block in jasmonic acid biosynthesis. *Plant J.* **31,** 1–12 (2002).
20. Vick, B. A. & Zimmerman, D. C. Lipoxygenase and hydroperoxide lyase in germinating watermelon seedlings. *Plant Physiol.* **57,** 780–788 (1976).
21. Grechkin, A. N. & Hamberg, M. The ''heterolytic hydroperoxide lyase'' is an isomerase producing a short-lived fatty acid hemiacetal. *Biochim. Biophys. Acta* **1636,** 47–58 (2004).
22. Itoh, A. & Howe, G. A. Molecular cloning of a divinyl ether synthase. Identification as a CYP74 cytochrome P-450. *J. Biol. Chem.* **276,** 3620–3627 (2001).
23. Grechkin, A. N. Hydroperoxide lyase and divinyl ether synthase. *Prostaglandins Other Lipid Mediat.* **68–69,** 457–470 (2002).
24. Stumpe, M. & Feussner, I. Formation of oxylipins by CYP74 enzymes. *Phytochem. Rev.* **5,** 347–357 (2006).
25. Guengerich, F. P. Cytochrome P450 enzymes in the generation of commercial products. *Nat. Rev. Drug Discov.* **1,** 359–366 (2002).
26. Denisov, I. G., Makris, T. M., Sligar, S. G. & Schlichting, I. Structure and chemistry of cytochrome P450. *Chem. Rev.* **105,** 2253–2277 (2005).
27. Poulos, T. L. & Johnson, E. F. in *Cytochrome P450: Structure, Mechanism and Biochemistry* 3rd edn (ed. P.R. Ortiz de Montellano) 87–114 (Plenum, 2005).
28. Williams, P. A., Cosme, J., Sridhar, V., Johnson, E. F. & McRee, D. E. Mammalian microsomal cytochrome P450 monooxygenase: structural adaptations for membrane binding and functional diversity. *Mol. Cell* **5,** 121–131 (2000).
29. Froehlich, J. E., Itoh, A. & Howe, G. A. Tomato allene oxide synthase and fatty acid hydroperoxide lyase, two cytochrome P450s involved in oxylipin metabolism, are targeted to different membranes of chloroplast envelope. *Plant Physiol.* **125,** 306–317 (2001).
30. Vidi, P. A. *et al.* Tocopherol cyclase (VTE1) localization and vitamin E accumulation in chloroplast plastoglobule lipoprotein particles. *J. Biol. Chem.* **281,** 11225–11234 (2006).
31. Joo, H., Lin, Z. & Arnold, F. H. Laboratory evolution of peroxide-mediated cytochrome P450 hydroxylation. *Nature* **399,** 670–673 (1999).
32. Bell, C. D., Soltis, D. E. & Soltis, P. S. The age of the angiosperms: a molecular timescale without a clock. *Evolution Int. J. Org. Evolution* **59,** 1245–1258 (2005).
33. White, R. E. & Coon, M. J. Oxygen activation by cytochrome P-450. *Annu. Rev. Biochem.* **49,** 315–356 (1980).
34. Smith, D. M., Nicolaides, A., Golding, B. T. & Radom, L. Ring opening of the cyclopropylcarbinyl radical and its N- and O-substituted analogs: A theoretical examination of very fast unimolecular reactions. *J. Am. Chem. Soc.* **120,** 10223–10233 (1998).
35. Groves, J. T. The bioinorganic chemistry of iron in oxygenases and supramolecular assemblies. *Proc. Natl Acad. Sci. USA* **100,** 3569–3574 (2003).
36. Green, M. T., Dawson, J. H. & Gray, H. B. Oxoiron(IV) in chloroperoxidase compound II is basic: implications for P450 chemistry. *Science* **304,** 1653–1656 (2004).
37. Ogliaro, F., de Visser, S. P. & Shaik, S. The 'push' effect of the thiolate ligand in cytochrome P450: a theoretical gauging. *J. Inorg. Biochem.* **91,** 554–567 (2002).
38. Koljak, R., Boutaud, O., Shieh, B. H., Samel, N. & Brash, A. R. Identification of a naturally occurring peroxidase–lipoxygenase fusion protein. *Science* **277,** 1994–1996 (1997).
39. Oldham, M. L., Brash, A. R. & Newcomer, M. E. The structure of coral allene oxide synthase reveals a catalase adapted for metabolism of a fatty acid hydroperoxide. *Proc. Natl Acad. Sci. USA* **102,** 297–302 (2005).
40. Lohelaid, H. *et al.* Identification of a functional allene oxide synthase–lipoxygenase fusion protein in the soft coral *Gersemia fruticosa* suggests the generality of this pathway in octocorals. *Biochim. Biophys. Acta* **1780,** 315–321 (2008).
41. Schneider, C. *et al.* Enzymatic synthesis of a bicyclobutane fatty acid by a hemoprotein lipoxygenase fusion protein from the cyanobacterium Anabaena PCC 7120. *Proc. Natl Acad. Sci. USA* **104,** 18941–18945 (2007).
42. Nelson, D. R. Plant cytochrome P450s from moss to poplar. *Phytochem. Rev.* **5,** 193–204 (2006).
43. Rensing, S. A. *et al.* The *Physcomitrella* genome reveals evolutionary insights into the conquest of land by plants. *Science* **319,** 64–69 (2008).
44. Cartwright, P. & Collins, A. Fossils and phylogenies: integrating multiple lines of evidence to investigate the origin of early metazoan lineages. *Integr. Comp. Biol.* **47,** 744–751 (2007).
45. Zabetakis, I. Enhancement of flavour biosynthesis from strawberry (*Fragraria ananassa*) callus cultures by *Methylobacterium* species. *Plant Cell Tissue Organ Cult.* **50,** 179–183 (1997).
46. Van Loon, L. C. & Bakker, P. A. in *Plant-associated Bacteria* (ed. Gnanamanickam, S. S.) 269–316 (Springer, 2006).
47. Beckers, G. J. & Conrath, U. Priming for stress resistance: from the lab to the field. *Curr. Opin. Plant Biol.* **10,** 425–431 (2007).
48. Renier, A. *et al.* Symbiotic properties of *Methylobacterium nodulans* ORS 2060T: A classic process for an atypical symbiont. *Soil Biol. Biochem.* **40,** 1404–1412 (2008).
49. Jourand, P. *et al.* Role of methylotrophy during symbiosis between *Methylobacterium nodulans* and *Crotalaria podocarpa*. *Mol. Plant Microbe Interact.* **18,** 1061–1068 (2005).
50. Brash, A. R., Yu, Z., Boeglin, W. E. & Schneider, C. The hepoxilin connection in the epidermis. *FEBS J.* **274,** 3494–3502 (2007).

Supplementary Information is linked to the online version of the paper at www.nature.com/nature.

Acknowledgements C.S.R. is grateful to the late N. Natarajaratnam and the late T. Traylor for encouragement; R. Cudney for nonanoyl-*N*-hydroxyethylglucamide (HEGA-9); K. Matsui for tomato *HPL* complementary DNA; K. Back and D. Park for *Arabidopsis* and rice cDNA libraries; L. Holland and J. Langeland for the amphioxus cDNA library; M. Medina for *A. palmata* expressed sequence tags; C. Marx and L. Moulin for *M. nodulans* cells; R. Müller for *S. aurantiaca* genomic DNA; L. Roman and B. Masters for the pCW_{ori}^{+} vector; J. Navarro for the single crystal microspectrophotometer; T. Doukov, S. Soltis, A. Cohen and J. Charles for help with acquiring electronic absorption spectra of single crystals; S. Veeraraghavan for generating Fig. 5; R. Bach, T. Bach, A. Beckwith, W. Bernhard, D. Curran, A. Davies, T. Dibble, J. Finnerty, D. Fleischman, J. Froehlich, J. Groves, L. Holland, P. Holland, J. Howieson, H. Kaplan, D. Nelson, M. Newcomb, P. Ortiz de Montellano, N. Porter, T. Poulos, M. Sibi, S. Veeraraghavan and D. Whalen for discussions; Joint Genome Institute for access to sequence data; Stanford Synchrotron Radiation Laboratories (beam lines 9–2 and 11–1, T. Doukov and L. Dunn) and the Advanced Light Source (beam line 8.3.1, J. Holton, G. Meigs and J. Tanamachi; beam lines 8.2.1 and 8.2.2, C. Ralston) for beam time and assistance. This work is supported by Pew Charitable Trusts through a Pew Scholar Award (C.S.R.), The Robert A. Welch Foundation (C.S.R.), The National Institutes of Health (C.S.R.), a Beginning Grant in Aid from the American Heart Association (D.-S.L.), and an INSERM Avenir Grant sponsored by La Fondation pour la Recherche Médicale (P.N.).

Author Contributions C.S.R. designed the research. D.-S.L. overexpressed and purified all the proteins used in this work; D.-S.L. and P.N. measured enzyme kinetic data; D.-S.L. generated the crystals; D.-S.L. and C.S.R. collected X-ray diffraction data; P.N. and C.S.R. solved the structures; P.N. did structure refinements; C.S.R. carried out bioinformatic and phylogenetic analyses; M.H. performed GC–MS and radio-HPLC measurements, and determined the structures of the reaction products; and C.S.R. wrote the paper. All authors discussed the results and commented on the manuscript.

Author Information Coordinates and structure factors have been deposited in the RCSB Protein Data Bank under the following accession codes: 3CLI (At-AOS), 3DSI (At-AOS in complex with 13-HOT), 2RCH (At-AOS in complex with 13-HOD), 2RCL (At-AOS in complex with 12*R*,13*S*-vernolic acid), 2RCM (At-AOS(F137L)), 3DSJ (At-AOS(F137L) in complex with 13-HOD), and 3DSK (At-AOS(F137L) in complex with 12*R*,13*S*-vernolic acid). Nucleotide sequences of Ap-AOS, Bf-EAS and Mn-HPL have been deposited in Genbank under accession numbers EU541487, EU555186 and EU887514, respectively. Reprints and permissions information is available at www.nature.com/reprints. Correspondence and requests for materials should be addressed to C.S.R. (ramancs@gmail.com).

METHODS

Protein expression and purification. We used the Johnson–Waterman method[51–54] to overproduce all the cytochromes P450 and their variants described in this work. *AOS* gene was PCR-amplified using *A. thaliana* and *O. sativa* cDNA libraries (gift from K. W. Back and D. S. Park) as templates. *Lycopersicon esculentum* (tomato) *HPL* cDNA was a gift from K. Matsui. For overexpression of At-AOS (Genbank accession number: Q96242) in *E. coli*, we generated an insert that lacks the first 32 residues, encompassing the chloroplast targeting peptide[55]. We also added seven residues (MAKKTSS) to the N terminus for improving protein solubility and a C-terminal tetra-histidine tag to facilitate purification. *O. sativa* (rice) AOS (Genbank accession number: AAL17675) and *L. esculentum* HPL (Genbank accession number: AAF67142) amplicons were generated in the same manner, but with the exception that only 21 N-terminal residues were removed. Bacterial and animal CYP74 orthologues were overproduced with intact N-termini. *Methylobacterium nodulans* HPL was PCR amplified from bacterial cells provided by C. Marx and L. Moulin. *Branchiostoma floridae EAS* was PCR amplified using cDNA library[56] (gift from L. Holland and J. Langeland) as the template. This insert includes the C-terminal LH2 domain. An expressed sequence tag (GENBANK accession number: DR983439; EST name: JGI_AOKF1116.fwd; gift from M. Medina) was used to clone *Acropora palmata* AOS. All inserts were ligated into the $pCW_{ori}+$ vector (gift of L. Roman and B. S. Masters), sequence verified (Lone Star Labs), and transformed into *Escherichia coli* BL21(DE3) cells. Post induction, the cells were harvested and the lysate was used in subsequent purification steps. The choice of detergent was empirically determined by means of screening and optimization. We adapted the Johnson method[54] to purify the P450s in three steps: (1) affinity chromatography (Ni-NTA, Qiagen) in the presence of 0.6–1% *n*-octyl-β-D-glucopyranoside (Anatrace); (2) ion exchange chromatography; and (3) gel filtration (Superdex 200 16/60; GE HealthCare). Haem content was assessed by means of pyridine hemochrome measurements[57]. Labelled protein was purified in a similar manner except that the cells were grown in minimal media supplemented with selenomethionine. Before crystallization At-AOS was detergent exchanged into nonanoyl-*N*-hydroxyethylglucamide (HEGA-9).

S. aurantiaca allene oxide cyclase (*AOC*) was PCR amplified from genomic DNA (gift from R. Müller). For overproduction and purification, we adapted methods described for *Arabidopsis* AOC[58].

Activity measurements. AOS, HPL and their variants (0.2–4 μM) were incubated with hydroperoxides (200 μM) at 23 °C for 15 min. Part of the reaction product was treated with 3 vol of 30 mM *O*-methylhydroxylamine in methanol at 23 °C for 2 h to generate *O*-methyloxime derivatives of short-chain aldehydes and other carbonyl-containing oxylipins. Additional derivatization of products extracted with diethyl ether was performed by consecutive treatments with ethereal diazomethane and a 2:1:2 (vol/vol/vol) mixture of trimethylchlorosilane, hexamethyldisilazane and pyridine to generate methyl esters from carboxylic acids and trimethylsilyl ethers from alcohols, respectively. As a control, hydroperoxides were also incubated with preparations of native maize AOS[59], garlic DES[60] and guava HPL[61].

Oxylipin profiles generated from the incubation of hydroperoxides with CYP74 enzymes were determined by GC–MS analysis run in the scan mode (*m*/*z* 50–600) and using the authentic compounds as references (Lipidox Co.). The selected ion monitoring (sim) mode was used for sensitive and specific detection. For analysis of oxylipins the following ions and compounds were used. 13-HPOD-derived products: *m*/*z* 412, 13-hydroxy-12-oxo-9(*Z*)-octradecenoic acid (AOS); *m*/*z* 308, etheroleic acid (DES); *m*/*z* 224, 12-oxo-9(*Z*)-dodecenoic acid (HPL). 9-HPOD-derived products: *m*/*z* 412, 9-hydroxy-10-oxo-12(*Z*)-octadecenoic acid (AOS); *m*/*z* 308, colneleic acid (DES); *m*/*z* 184 and 152, 9-oxononanoic acid (HPL). 13-HPOT-derived products: *m*/*z* 410, 13-hydroxy-12-oxo-9(*Z*),15(*Z*)-octadecadienoic acid (AOS); *m*/*z* 306, 12-oxophytodienoic acid (AOS); *m*/*z* 306, etherolenic acid (DES); *m*/*z* 224, 12-oxo-9(*Z*)-dodecenoic acid (HPL). 11-HPHT-derived products: *m*/*z* 382, 11-hydroxy-10-oxo-7(*Z*),13(*Z*)-hexadecadienoic acid; *m*/*z* 278, dinor-12-oxophytodienoic acid (AOS); *m*/*z* 278, dinor-etherolenic acid (DES); and *m*/*z* 196, 10-oxo-7(*Z*)-decenoic acid (HPL). The abundance of products generated in the various incubations was estimated by integration of the intensities of mass spectral ions.

Oxylipin production by recombinant CYP74 enzymes from *M. nodulans*, *A. palmata* and *B. floridae* was measured by radio-HPLC methods. Initially, 0.2–4 μM of the enzyme was incubated with [1-^{14}C]13(*S*)-HPOD (200 μM) at 23 °C for 15 min. This was followed by derivatization of carbonyl groups with 30 mM *O*-methyl hydroxylamine in methanol at room temperature (23 °C) for 2 h. After solvent extraction and methyl-esterification, normal phase HPLC was performed using 0.6% 2-propanol-hexane (0–15 min) and 1.2% 2-propanol-hexane (15–35 min) for elution.

Enzyme kinetics. Hydroperoxide consumption by AOS and its mutants was quantified using ultraviolet spectrophotometry[62], by following the decrease in absorption at 235 nm stemming from the loss of conjugated diene system of the substrate. Reactions were performed at 23 °C in 0.5 ml of 50 mM sodium phosphate buffer, pH 7. Initial velocity measurements used fixed enzyme concentration (wild-type AOS, 6 nM; Phe to Leu mutants, 1.5 nM; and At-AOS(N321Q), 30 nM) while varying the 13(*S*)-HPOD concentration. Activity slopes were obtained under initial velocity conditions, in which less than 10% of the substrate has been converted into product.

Crystallization and data collection. Crystals were obtained by the sitting-drop vapour diffusion method at 20 °C. At-AOS crystals were grown from 100 mM Tris-HCl, pH 7.5, 15–20% polyethylene glycol (PEG) 3350, and 39 mM HEGA-9. Substrate and intermediate analogues were premixed with the protein solution before generating crystals of the complexes. Streak seeding was used to grow crystals of AOS variants.

Because X-rays are capable of reducing the haem iron during data collection[63], we have used three distinct strategies for minimizing X-ray damage to crystals: (1) use a data collection strategy that generates a complete diffraction data set from a single crystal with the least amount of X-ray exposure (for example, in the At-AOS case we were able to collect the entire data set within 2 min with each frame being exposed for only 0.5 s; total dose received = 3.8×10^5 grey or 2% of Henderson limit); (2) perform data collection at a shorter wavelength (below 0.83 Å)[64]; (3) use single crystals that were co-crystallized in the presence of 10 mM potassium ferricyanide[65]. Visible absorption spectra of At-AOS crystals were obtained using a microspectrophotometer setup (4DXray Systems) adapted for use at the Stanford Synchrotron Radiation Laboratories.

Diffraction data were collected (100 K) at SSRL BL 9–2, BL 11–1, and ALS BL 8.3.1, BL 8.2.1 and BL 8.2.2. Glycerol was used as the cryoprotectant. Single wavelength anomalous diffraction and multiwavelength anomalous diffraction data sets were collected at the iron and selenium edges (Supplementary Tables 1 and 2). Data were integrated and scaled with MOSFLM[66]/SCALA[67] or HKL2000 (ref. 68).

Structure determination and refinement. Se-MAD data was used to obtain phase information. SHELXS[69] was used to locate the anomalous scatterers (16 Se). Refinement of heavy-atom parameters and phase calculation were done using SHARP[70]. Solvent flattening with SOLOMON[71] and phase extension yielded electron density maps into which most residues were built with the program O[72]. The model was further refined with REFMAC5 (ref. 73) using a maximum-likelihood target function and translation/libration/screw refinement[74]. Subsequent model building allowed us to generate the complete model (Supplementary Tables 1 and 2). Structures of ligand-bound complexes were obtained by means of difference Fourier methods. Figures were generated using PYMOL[75].

51. Barnes, H. J., Arlotto, M. P. & Waterman, M. R. Expression and enzymatic activity of recombinant cytochrome P450 17 α-hydroxylase in *Escherichia coli*. *Proc. Natl Acad. Sci. USA* **88,** 5597–5601 (1991).
52. Richardson, T. H. *et al.* Purification and characterization of recombinant-expressed cytochrome P450 2C3 from *Escherichia coli*: 2C3 encodes the 6 β-hydroxylase deficient form of P450 3b. *Arch. Biochem. Biophys.* **300,** 510–516 (1993).
53. von Wachenfeldt, C., Richardson, T. H., Cosme, J. & Johnson, E. F. Microsomal P450 2C3 is expressed as a soluble dimer in *Escherichia coli* following modification of its N-terminus. *Arch. Biochem. Biophys.* **339,** 107–114 (1997).
54. Wester, M. R., Stout, C. D. & Johnson, E. F. Purification and crystallization of N-terminally truncated forms of microsomal cytochrome P450 2C5. *Methods Enzymol.* **357,** 73–79 (2002).
55. Hughes, R. K. *et al.* Allene oxide synthase from *Arabidopsis thaliana* (CYP74A1) exhibits dual specificity that is regulated by monomer–micelle association. *FEBS Lett.* **580,** 4188–4194 (2006).
56. Langeland, J. A., Tomsa, J. M., Jackman, J. W. R. & Kimmel, C. B. An amphioxus snail gene: expression in paraxial mesoderm and neural plate suggests a conserved role in patterning the chordate embryo. *Dev. Genes Evol.* **208,** 569–577 (1998).
57. Berry, E. A. & Trumpower, B. L. Simultaneous determination of hemes a, b, and c from pyridine hemochrome spectra. *Anal. Biochem.* **161,** 1–15 (1987).
58. Hofmann, E., Zerbe, P. & Schaller, F. The crystal structure of *Arabidopsis thaliana* allene oxide cyclase: insights into the oxylipin cyclization reaction. *Plant Cell* **18,** 3201–3217 (2006).
59. Hamberg, M. & Fahlstadius, P. Allene oxide cyclase: a new enzyme in plant lipid metabolism. *Arch. Biochem. Biophys.* **276,** 518–526 (1990).
60. Grechkin, A. N., Fazliev, F. N. & Mukhtarova, L. S. The lipoxygenase pathway in garlic (*Allium sativum* L.) bulbs: detection of the novel divinyl ether oxylipins. *FEBS Lett.* **371,** 159–162 (1995).
61. Grechkin, A. N. & Hamberg, M. The "heterolytic hydroperoxide lyase" is an isomerase producing a short-lived fatty acid hemiacetal. *Biochim. Biophys. Acta* **1636,** 47–58 (2004).
62. Brash, A. R. & Song, W. C. Detection, assay, and isolation of allene oxide synthase. *Methods Enzymol.* **272,** 250–259 (1996).

63. Beitlich, T., Kuhnel, K., Schulze-Briese, C., Shoeman, R. L. & Schlichting, I. Cryoradiolytic reduction of crystalline heme proteins: analysis by UV-Vis spectroscopy and X-ray crystallography. *J. Synchrotron Radiat.* **14,** 11–23 (2007).
64. Schlichting, I. Crystallographic structure determination of unstable species. *Acc. Chem. Res.* **33,** 532–538 (2000).
65. Lancaster, C. R., Kroger, A., Auer, M. & Michel, H. Structure of fumarate reductase from *Wolinella succinogenes* at 2.2 A resolution. *Nature* **402,** 377–385 (1999).
66. Leslie, A. G. W. Joint CCP4 + ESF-EAMCB Newsletter on Protein Crystallograpy, No. 26. (Warrington, UK, Daresbury Lab, 1992).
67. Collaborative Computational Project Number 4.. The CCP4 suite programs for protein crystallography. *Acta Crystallogr. D* **50,** 760–763 (1994).
68. Otwinowski, Z. & Minor, W. Processing of X-ray diffraction data collected in oscillation mode. *Methods Enzymol.* **276,** 307–325 (1997).
69. Sheldrick, G. M. Patterson superpositioning and ab initio phasing. *Methods Enzymol.* **276,** 628–641 (1997).
70. de La Fortelle, E. & Bricogne, G. Maximum-likelihood heavy atom parameter refinement for multiple isomorphous replacement and multiwavelength anomalous diffraction methods. *Methods Enzymol.* **276,** 472–494 (1997).
71. Abrahams, J. P. & Leslie, A. G. Methods used in the structure determination of bovine mitochondrial F1 ATPase. *Acta Crystallogr. D* **52,** 30–42 (1996).
72. Jones, T. A., Zou, J. Y., Cowan, S. W. & Kjeldgaard, M. Improved methods for building protein models into electron density maps and the location of errors in these models. *Acta Crystallogr.* **A47,** 110–119 (1991).
73. Murshudov, G. N., Vagin, A. A. & Dodson, E. J. Refinement of macromolecular structures by the maximum-likelihood method. *Acta Crystallogr. D* **53,** 240–255 (1997).
74. Winn, M. D., Isupov, M. N. & Murshudov, G. N. Use of TLS parameters to model anisotropic displacements in macromolecular refinement. *Acta Crystallogr. D* **57,** 122–133 (2001).
75. DeLano, W. L. The PyMOL Molecular Graphics System <http://www.pymol.org> (DeLano Scientific, 2002).